Cancer Cell
Article

An Antioxidant Response Phenotype Shared between Hereditary and Sporadic Type 2 Papillary Renal Cell Carcinoma

Aikseng Ooi,[1] Jing-Chii Wong,[2] David Petillo,[1] Douglas Roossien,[1] Victoria Perrier-Trudova,[1,3] Douglas Whitten,[4] Bernice Wong Hui Min,[2] Min-Han Tan,[2] Zhongfa Zhang,[1,9] Ximing J. Yang,[5] Ming Zhou,[6] Betty Gardie,[3] Vincent Molinié,[3] Stéphane Richard,[3] Puay Hoon Tan,[7] Bin Tean Teh,[1,2,*] and Kyle A. Furge[8,*]
[1]Laboratory of Cancer Genetics, Van Andel Research Institute, Grand Rapids, MI 49503, USA
[2]NCCS-VARI Translational Cancer Research Laboratory, National Cancer Centre Singapore, 169610 Singapore
[3]Génétique Oncologique EPHE-INSERM U753 and Faculté de Médecine Paris-Sud, Le Kremlin-Bicêtre, and Institut de Cancérologie Gustave Roussy, 94805 Villejuif, France
[4]Proteomics Core Facility, Michigan State University, East Lansing, MI 48824, USA
[5]Department of Pathology, Northwestern Memorial Hospital, Northwestern University Feinberg School of Medicine, Chicago, IL 60611, USA
[6]Department of Anatomic Pathology, Cleveland Clinic, Cleveland, OH 44195, USA
[7]Department of Pathology, Singapore General Hospital, 169608 Singapore
[8]Laboratory of Computational Biology, Van Andel Research Institute, Grand Rapids, MI 49503, USA
[9]Present address: Center for Systems and Computational Biology, The Wistar Institute, Philadelphia, PA 19104, USA
*Correspondence: bin.teh@vai.org (B.T.T.), kyle.furge@vai.org (K.A.F.)
DOI 10.1016/j.ccr.2011.08.024

SUMMARY

Fumarate hydratase (*FH*) mutation causes hereditary type 2 papillary renal cell carcinoma (PRCC2). The main effect of *FH* mutation is fumarate accumulation. The current paradigm posits that the main consequence of fumarate accumulation is HIF-α stabilization. Paradoxically, *FH* mutation differs from other HIF-α stabilizing mutations, such as *VHL* and *SDH* mutations, in its associated tumor types. We identified that fumarate can directly up-regulate antioxidant response element (ARE)–controlled genes. We demonstrated that aldo-keto reductase family 1 member B10 (*AKR1B10*) is an ARE-controlled gene and is up-regulated upon FH knockdown as well as in *FH* null cell lines. *AKR1B10* overexpression is also a prominent feature in both hereditary and sporadic PRCC2. This phenotype better explains the similarities between hereditary and sporadic PRCC2.

INTRODUCTION

Type 2 papillary renal cell carcinoma (PRCC2) is an aggressive subtype of kidney cancer that has no effective treatment. The hereditary form is associated with biallelic inactivation of the gene encoding the Kreb's cycle enzyme fumarate hydratase (*FH*), which causes hereditary leiomyomatosis and renal cell cancer (HLRCC) (MIM ID #605839) that is characterized by kidney cancer, uterine fibroids, and cutaneous leiomyomatosis at high frequencies (Launonen et al., 2001; Tomlinson et al., 2002). Individuals who have HLRCC are also genetically predisposed to bladder cancer, collecting-duct tumors, and adult Leydig cell tumors of the testis (Alam et al., 2003; Carvajal-Carmona et al., 2006; Kiuru and Launonen, 2004; Lehtonen et al., 2006).

The current paradigm is that *FH* mutation causes the stabilization and accumulation of hypoxia-inducible factor alpha subunit (HIF-α), as well as increased expression of HIF-α target genes, such as vascular endothelial growth factor (*VEGFA*) and platelet-derived growth factor (*PDGF*) (Isaacs et al., 2005; Koivunen et al., 2007; O'Flaherty et al., 2010). However, this paradigm fails to explain the distinct clinical, biochemical, and genetic features apparent between tumors harboring *FH* mutation and

Significance

Type 2 papillary renal cell carcinoma (PRCC2) is an aggressive disease with no effective treatment. Despite the obvious morphological, genetic, and clinical differences, hereditary PRCC2 is thought to share similar pathway deregulation with its clear-cell counterpart (CCRCC) that arises as a result of *SDH* or *VHL* mutation. Furthermore, the robust response seen with anti-VEGF agents in CCRCC is not reproducible in PRCC2. This represents a distinct knowledge gap in the understanding of PRCC2 biology. We identified deregulation of the KEAP1-NRF2 axis as a feature that distinguishes PRCC2 from CCRCC, but links both hereditary and sporadic PRCC2. Therefore, our finding provides a more complete understanding of PRCC2 biology and lays the foundation for the development of effective treatment strategies.

those harboring other HIF-α-accumulating mutations in genes such as von Hippel–Lindau (*VHL*) and succinate dehydrogenase (*SDH*). Both *VHL* and *SDH* mutations are associated with clear-cell renal cell carcinoma (CCRCC), pheochromocytoma, and paraganglioma (Vanharanta et al., 2004). Clinically, the robust response of CCRCC to antiangiogenic agents that block VEGFA has not been seen in either sporadic or hereditary PRCC2 (Molina et al., 2010). Furthermore, HIF-α-associated histology such as higher vascular density is more apparent in hereditary PRCC2 (Pollard et al., 2005a), suggesting that this model fails to adequately describe the similarities between hereditary and sporadic PRCC2.

The homeostasis of HIF-α is controlled at the protein level. Under normoxic conditions, HIF-α is hydroxylated by prolyl hydroxylase, marking it for ubiquitination by an E3 ubiquitin ligase complex that contains VHL (Ivan et al., 2001). In cells devoid of VHL function, the E3 ubiquitin ligase complex fails to form and HIF-α accumulates. In cells lacking SDH function, succinate accumulates and inhibits HIF-α prolyl hydroxylase in a competitive manner (Pollard et al., 2006). *VHL* and *SDH* mutations caused a similar spectrum of tumors. Overexpression of HIF-α target genes is also a common feature of tumors harboring either mutated gene (Dahia et al., 2005).

The accumulation of HIF-α resulting from *FH* mutation is believed to be mediated by fumarate inhibition of prolyl hydroxylase, in a manner similar to that of succinate (Isaacs et al., 2005; Koivunen et al., 2007; O'Flaherty et al., 2010). FH catalyzes the hydration of fumarate to malate in the Kreb's cycle, and its loss causes the accumulation of fumarate and succinate (Pollard et al., 2005b). Both can escape into the cytosol, and the former is believed to drive the development of HLRCC symptoms and complications (Pollard et al., 2005b). An alternative theory is that HIF-α accumulates as reactive oxygen species (ROS) increase, which results from a glycolytic switch due to Kreb's cycle failure when *FH* is mutated (Sudarshan et al., 2009).

We sought a model that better describes both hereditary PRCC2 (hereafter, HLRCC) and sporadic PRCC2 (hereafter, PRCC2) through comprehensive analysis of transcriptome data.

RESULTS

The Expression Pattern of HIF-α-Associated Proangiogenic Factors Differentiate CCRCC from HLRCC and PRCC2

It is well accepted that HIF-α is stabilized and that its target genes are overexpressed in HLRCC and CCRCC (reviewed in Linehan et al., 2010). It has also been shown that pheochromocytomas, arising from either *VHL* or *SDH* mutation, have HIF-α accumulation (Dahia et al., 2005). To assess the differences in HIF-α-mediated transcription changes in RCC subtypes, we used gene expression data sets from pheochromocytoma samples that arose from MEN2A, *SDH*, and *VHL* mutations. We identified a set of genes commonly deregulated in pheochromocytomas harboring *VHL* or *SDH* mutation (see Table S1, which is available with this article online). Concordant with previously reported work, the gene expression profiles from *SDH* mutant pheochromocytomas were markedly similar to those derived from *VHL* mutation ($p = 1.026149 \times 10^{-22}$, mean-rank gene set test; Table S1 and Figure 1A).

Next, we identified genes commonly up-regulated in pheochromocytomas that had *SDH* or *VHL* mutations (Table S1) and performed functional annotation clustering to identify genes associated with the proangiogenic phenotype, common to SDH and VHL loss of function. We found a subset of 10 genes associated with angiogenesis ($p < 0.05$; enrichment score = 2.04) (Figure 1B); seven of those were coordinately overlapped with four angiogenesis GO terms. As expected, these seven genes were also overexpressed in CCRCC relative to normal kidney (Figure 1C), but their expression levels were not prominently changed in either PRCC2 or HLRCC (Figure 1C; the demographical and mutation status of HLRCC samples used in this study are shown in Table S2). In particular, the expression of *VEGFA* in PRCC2 and in HLRCC was much lower than in CCRCC. The VEGFA mRNA level was further validated by quantitative reverse transcription PCR (qRT-PCR), and the result agreed with that from our microarray (Figure S1). A similar analysis on proglycolytic features of HLRCC tumors showed overexpression of other HIF-α target genes such as hexokinase 2 and glucose transporter type 1 (data not shown).

Gene Expression Signature Manifests the Loss of FH Function in Sporadic PRCC2

The divergence in the expression of HIF-α-associated proangiogenic genes among CCRCC, HLRCC, and PRCC2 suggests that there may be deregulation of other pathways in papillary tumors. We generated an FH loss-of-function gene signature by using expression profiles previously generated from uterine fibroids harboring *FH* mutations (Vanharanta et al., 2006). We identified 94 up-regulated and 76 down-regulated genes (minimum twofold difference between $FH^{-/-}$and $FH^{+/+}$ fibroids; Figure 2A and Table S3). A similar analysis found 1397 up-regulated and 985 down-regulated genes in HLRCC relative to normal kidney tissues (Figure 2A and Table S3).

To cancel out tissue- and experiment-specific variations in gene expression, we compared these two lists and identified 44 genes up-regulated in both $FH^{-/-}$ fibroids and HLRCC and 26 genes down-regulated in both (Figure 2A and Table S3); this set was designated as the "FH signature." As expected, when the FH signature was used to interrogate the uterine fibroid data via gene set enrichment analysis, the signature was specifically enriched in $FH^{-/-}$ fibroid tissues (Figure 2B, left). In the same test on an independent set (GSE2725) of $FH^{-/-}$ and $FH^{+/+}$ uterine fibroids and normal myometrial tissues, the signature was again specifically enriched in $FH^{-/-}$ fibroids (Figure 2B, right). The FH signature was also enriched in $FH^{+/-}$ normal kidney (Figure 2C), suggesting that heterozygous *FH* mutation does alter the overall gene expression profile, possibly through accumulation of fumarate. A change in the gene expression profile of normal epithelial cells harboring heterozygous *BRCA1* or *BRCA2* mutations was recently reported (Bellacosa et al., 2010).

After validating the FH signature, we applied it to the PRCC2 data set and found that the signature was significantly enriched ($p = 3.60 \times 10^{-9}$) (Figure 2D). Twenty-one genes overlapped between the 2057 genes up-regulated in PRCC2 and the 44 up-regulated in our FH signature; 14 of 2251 genes down-regulated in PRCC2 also overlapped ($p = 4.02 \times 10^{-10}$ and 6.84×10^{-08} for up- and down-regulation, respectively) (Figure 2E).

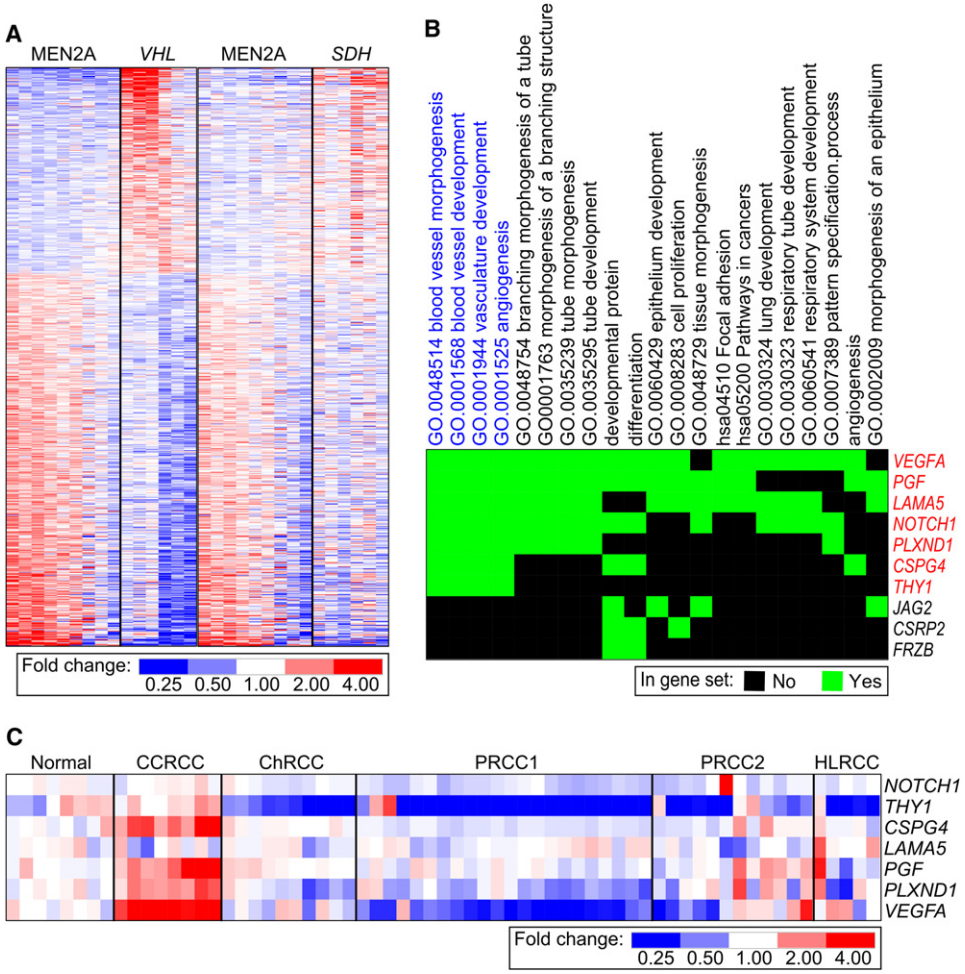

Figure 1. HIF-α-Associated Proangiogenic Factors of HLRCC and PRCC2 Differ from Those of CCRCC

(A) Heat map showing fold change of mRNA from 778 differentially regulated genes in pheochromocytomas harboring MEN2A, *VHL*, or *SDH* mutations. Red and blue respectively represent higher and lower expression relative to the mean gene expression levels.

(B) Ten genes significantly associated with angiogenesis processes ($p < 0.05$; enrichment score = 2.04). Genes in red were coordinately overlapped with four angiogenesis GO terms (blue).

(C) Relative fold change in mRNA abundance of individual angiogenic genes in kidney cancers subtypes (ChRCC = chromophobe renal cell carcinoma) relative to the mean abundance in normal kidney tissues. See also Figure S1, Table S1, and Table S2.

Among the 21 up-regulated genes, the aldo-keto reductase family 1 member B10 gene (*AKR1B10*) was the most up-regulated, suggesting that there is a signal transduction defect resulting in such *AKR1B10* expression in both PRCC2 and HLRCC (Figure 2F and Table S4).

AKR1B10 as a Gene Controlled by Antioxidant Response Element

We used an algorithm that predicts *cis*-acting elements to identify potential transcription factors that control *AKR1B10* expression (Figure S2). By coalescing *cis*-acting element motifs associated with the *AKR1B10* expression pattern, we isolated 13 candidates (Figure S2 and Figure 3A). Three of these elements corresponded to sequences recognized by the nuclear factor (erythroid-derived 2)-like 1 (NRF1) and nuclear factor (erythroid-derived 2)-like 2 (NRF2) transcription factors, whereas two others correspond to JUN, which is known to dimerize with NRF and enable binding to a response element (Figure 3B) (Venugopal and Jaiswal, 1998). Collectively, these *cis*-acting elements correspond to the antioxidant response element (ARE) as being a potential controller of *AKR1B10* expression.

If this prediction is true, the expression pattern of *AKR1B10* should correlate with those of other classic ARE-driven genes. Thus, we performed a rank test on the *AKR1B10* expression pattern with the classic ARE-driven genes NAD(P)H dehydrogenase, quinone 1 (*NQO1*), and thioredoxin reductase 1 (*TXNRD1*) (Hsieh et al., 2006; Sakurai et al., 2005). As expected, the *AKR1B10* expression pattern correlated well with both *NQO1* and *TXNRD1* in the RCC data set, with Kendall correlation coefficients of 0.62 and 0.54, respectively (Pearson correlation coefficient > 0.7; $p < 0.05$ in all correlation plots) (Figures 3C and 3E). We also used independent data sets from lung small airway cells (GSE994) and obtained similar results (Kendall correlation coefficients of 0.67 and 0.50, respectively; Pearson

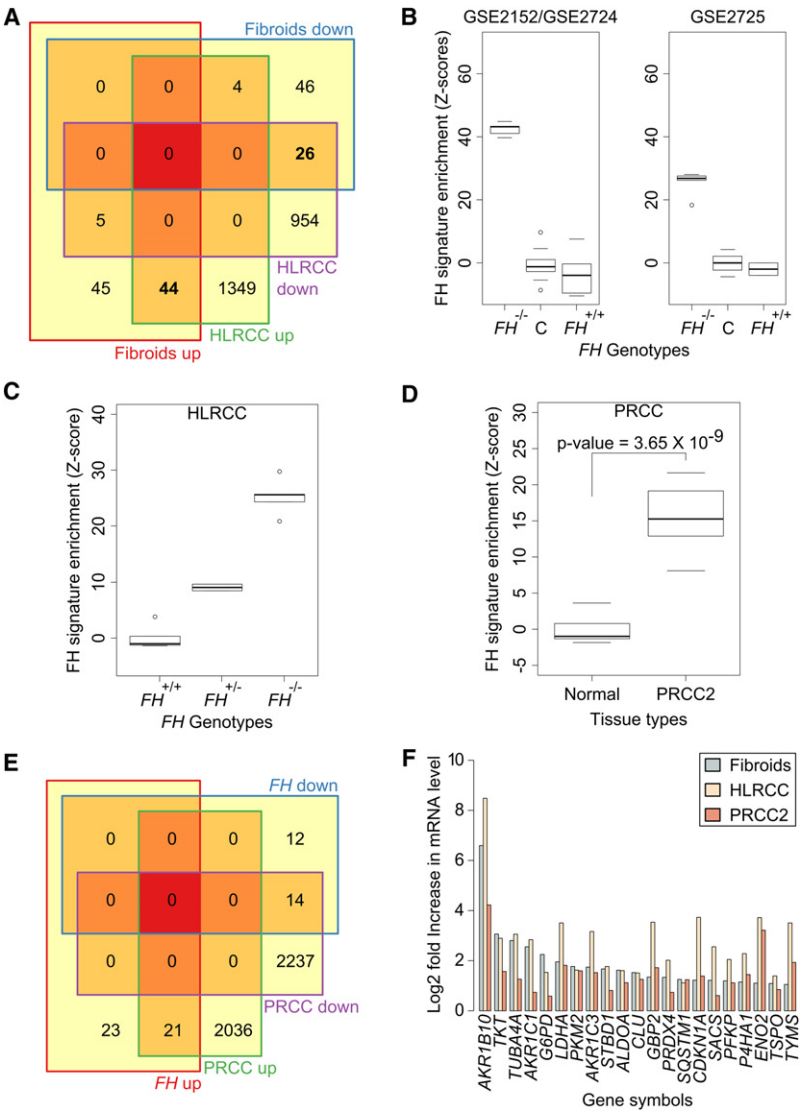

Figure 2. The FH Signature in Sporadic PRCC2

(A) Venn diagram of genes up- or down-regulated in $FH^{-/-}$ fibroids and HLRCC relative to $FH^{+/+}$ normal tissues. Bold designates the sets of up- and down-regulated genes subsequently used as the "*FH* signature."

(B) The FH signature was specifically enriched in $FH^{-/-}$ fibroids but not in normal myometria or $FH^{+/+}$ fibroid tissues.

(C) Enrichment of the FH signature in $FH^{+/+}$ normal kidney, $FH^{+/-}$ normal kidney, and $FH^{-/-}$ HLRCC tumor samples.

(D) FH signature enrichment in PRCC2 ($p = 3.60 \times 10^{-09}$).

(E) Venn diagram of genes up- and down-regulated in PRCC2 relative to normal tissue. The overlaps were statistically significant: with p values (hypergeometric test) of 4.02×10^{-10} and 6.84×10^{-8} for up- and down-regulated genes, respectively.

(F) Base 2 logarithmic fold increase in mRNA levels of the 21 commonly up-regulated genes in diseased tissues relative to corresponding controls. See also Tables S3 and S4.

correlation coefficient > 0.7; $p < 0.05$ in all correlation plots) (Figures 3D and 3F). Furthermore, we identified a potential ARE consensus sequence within the *AKR1B10* gene.

The FH Signature Significantly Overlaps the Gene Expression Profile of KEAP1 Knockdown

The ARE enhancer is recognized by NRF1 and NRF2 (Ohtsuji et al., 2008). These factors are negatively regulated by KEAP1 (although such regulation of NRF1 is not robustly established) (Furukawa and Xiong, 2005; Hayes and McMahon, 2001; Zhang et al., 2006). An electrophile sensor, KEAP1, binds to NRF transcription factors under low-electrophile conditions and brings them into close proximity with cullin 3 (CUL3) ubiquitin ligase for ubiquitination (Furukawa and Xiong, 2005; Zhang et al., 2005). The exposed cysteine residue of KEAP1, Cys-151, reacts with intracellular electrophiles (Rachakonda et al., 2008; Zhang and Hannink, 2003) by forming a covalent adduct, which induces a conformational change that renders KEAP1 unable to bind NRF2; thus, NRF2 accumulates and becomes available to modulate ARE-controlled genes.

We used expression data from a KEAP1 knockdown experiment to assess whether the KEAP1 inactivation profile shared features with our FH signature (MacLeod et al., 2009). Of the 66 up-regulated genes following KEAP1 knockdown, nine overlapped with the up-regulated portion of the FH signature (Figure 4A and Table S5); five of these nine were among the 20 most strongly up-regulated genes (Figure 4B) (hypergeometric $p = 6.70^{-16}$). The expression levels of the nine genes were consistently higher in $FH^{-/-}$ than in $FH^{+/+}$ uterine fibroids (Figure 4C); their expression levels in RCC subtypes are shown in Figure 4D. Consistent with their clinical and morphological features, the expression patterns of the nine genes were similar between HLRCC and PRCC2 and distinguished them from CCRCC. qRT-PCR validation on a subset of the nine genes is shown in Figure S3. The expression pattern of *AKR1B10* in data sets we used also correlated well with other NRF2 targets such as aldo-keto reductase family 1, member C1 (*AKR1C1*), glutamate-cysteine ligase, catalytic subunit (*GCLC*), and sulfiredoxin 1 (*SRXN1*), which have been identified as genes that become overexpressed upon KEAP1 knockdown (Figure S3) (MacLeod et al., 2009).

AKR1B10 mRNA Increased with Lower FH Level

Gene expression analysis suggested that AKR1B10 overexpression is a prominent feature of the loss of FH function and is likely an effect of NRF accumulation. To test this in a cellular system, we assessed AKR1B10, NRF1, NRF2, and KEAP1 protein levels in immortalized kidney tubular epithelial cells (HK-2) and an HLRCC cell line, UOK-262 (Yang et al., 2010). AKR1B10, NRF1, and NRF2 levels were higher in UOK-262 than in HK-2 cells (Figure 5A), whereas KEAP1 was lower. We then knocked down FH using two different species of siRNA in immortalized

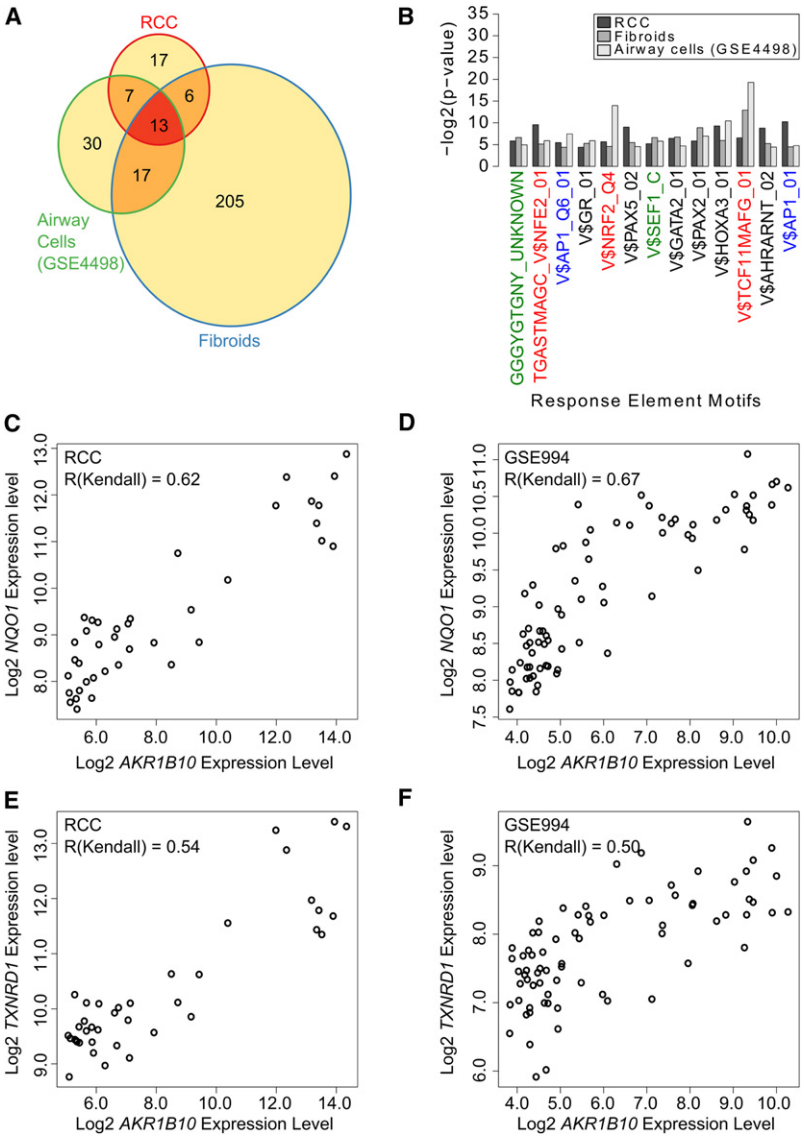

Figure 3. *cis*-Acting Element Motif Matching Algorithm Prediction That *AKR1B10* Is Controlled by ARE

(A) Venn diagram of *cis*-acting element motifs correlated to *AKR1B10* gene expression pattern in data sets from RCC (comprising normal kidney, PRCC1, and PRCC2), lung small airway cells, and fibroid.

(B) The $-\log_2$ p values (hypergeometric test) of the overlap between the *cis*-acting element motifs and the genes identified through Kendall Rank Test in three different data sets. Motif names in green were not assigned to any transcription factor; names in red represent the ARE; names in blue represent AP-1 or c-JUN binding sites. Collectively, red plus blue motifs correspond to the consensus motif of ARE.

(C–F) Correlation of the *AKR1B10* expression pattern with *NQO1* (C and D) and *TXNRD1* (E and F) in the RCC data set and in an independent data set from lung small airway cells. See also Figure S2.

embryonic kidney cells (HEK293) and HK-2 cells. We achieved over 60% knockdown of FH mRNA with each siRNA, but FH protein abundance decreased only moderately by 72 hr after knockdown (Figures 5B and 5C). This drop in FH protein was accompanied by an increase in NRF1 and NRF2 concentrations and a threefold increase in AKR1B10 mRNA relative to that using a scrambled siRNA control (Figure 5C). An experiment with non-immortalized PCS-400 primary kidney tubular epithelial cells produced similar results (Figure S4).

To further confirm the relationship between *FH* and *AKR1B10* expression, we reintroduced wild-type FH into the FH mutant line UOK-262 via lentivirus-mediated transgene knock-in. This gave reductions in intracellular fumarate, NRF2 protein, and AKR1B10 mRNA (Figure 5D).

The most immediate effect of losing FH function is the accumulation of intracellular fumarate (Pollard et al., 2005b). As expected, the intracellular fumarate level was also higher in the FH null cell line UOK262 relative to the FH wild-type lines HEK293 and HK-2 (Figure 5E). Knocking down *FH* in wild-type lines increased intracellular fumarate concentration, whereas knocking wild-type FH into UOK-262 decreased AKR1B10 mRNA (Figure 5E).

Fumarate Can Increase NRF1 and NRF2

We hypothesized that AKR1B10 overexpression is an effect of fumarate accumulation. Therefore, we simulated fumarate accumulation by exposing HK-2 cells to various concentrations of the membrane-permeable form, dimethyl fumarate (DMF), for 24 hr. The AKR1B10 mRNA level increased with DMF concentration in a dose-dependent manner (Figure 6A), and this increase was accompanied by an increase in NRF1 and NRF2 protein (Figure 6B). This effect was evident with only 12.5 μM DMF, a concentration far lower than that needed to stabilize HIF1α under similar culture conditions (Isaacs et al., 2005; Koivunen et al., 2007). Furthermore, reexpression of functional FH in the FH null lines reduced the intracellular fumarate, nuclear NRF2, and AKR1B10 expression levels (Figures 5D and 5E). These results support the prediction that fumarate is the electrophile sensed by KEAP1, which leads to the stabilization of NRF2 and in turn drives expression of *AKR1B10*.

The mechanism by which KEAP1 senses an electrophile allows its direct detection through mass spectrometry. Thus, we performed tandem mass spectrometry on HA-tagged human KEAP1 that was ectopically expressed in FH knockdown HEK293 cells and in scrambled-siRNA control cells. Cys-151 and Cys-288 of KEAP1 were modified by fumarate in FH knockdown cells (Figures 6C and 6D and Table S6). This modification is consistent with a nucleophilic addition reaction between fumarate and a cysteine sulfhydryl group, forming a 2-succinyl adduct. These modifications were not present in the scrambled-siRNA control. Additionally, a ubiquitination mark (GlyGly) was found on Lys-615 of KEAP1 isolated from FH knockdown cells (Figures S5A and S5B).

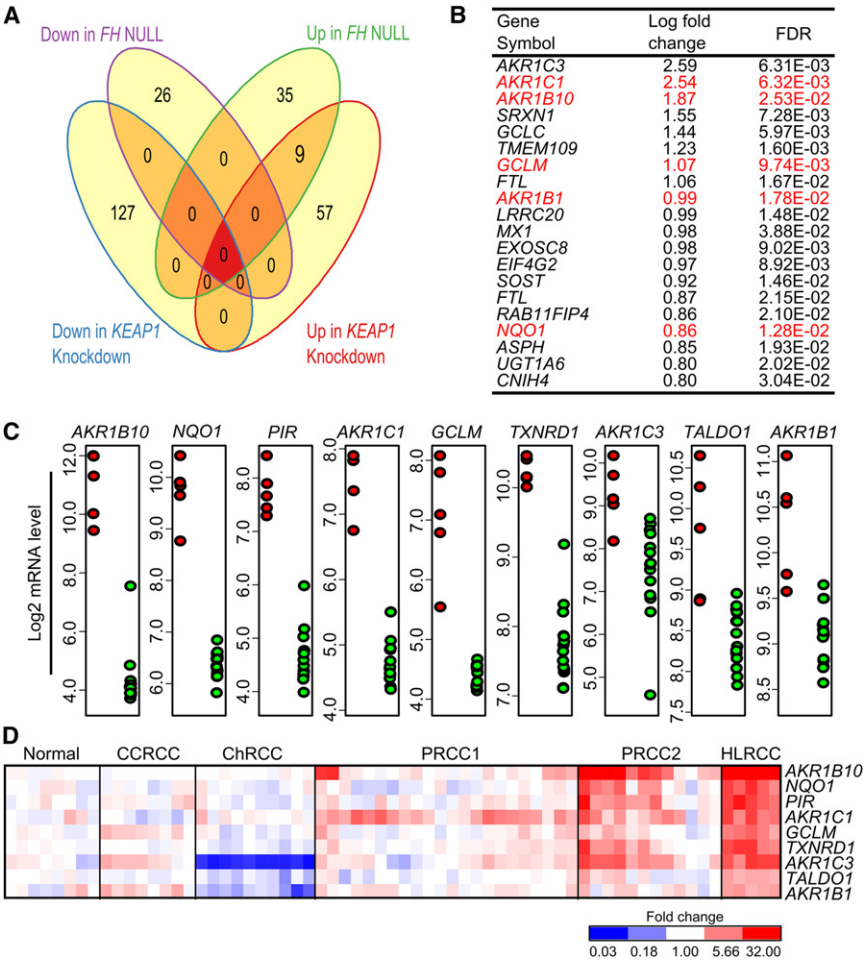

Figure 4. Genes Overexpressed upon KEAP1 Knockdown Overlap with Those upon Loss of *FH* Gene Function

(A) The number of overlapping genes between the FH signature and the genes overexpressed upon *KEAP1* knockdown; nine genes were overexpressed in common when either *FH* or *KEAP1* was knocked down.

(B) The 20 most highly overexpressed genes upon *KEAP1* knockdown. Genes in red were in the up-regulated component of the FH gene signature. This overlap is significant ($p = 6.70 \times 10^{-16}$ [hypergeometric test]).

(C) The relative mRNA levels of the nine overexpressed genes in $FH^{-/-}$ (red) and $FH^{+/+}$ (green) fibroids.

(D) The fold change in mRNA level for the nine overexpressed genes in RCC subtypes relative to the mean level in normal kidney. See also Figure S3 and Table S5.

Ubiquitination of KEAP1 upon modification of its cysteines by thiol-reactive compounds has been reported (Zhang et al., 2005). Our mass spectrometry results also suggest that succinated KEAP1 can become ubiquitinated. Furthermore, Western blots detected a higher abundance of ubiquitin on HA-tagged KEAP1 in FH knockdown cells than in scrambled siRNA-treated HEK293 cells (Figure S5C). The amount of ubiquitinated KEAP1 increased with proteasome inhibitor (MG132) treatment, suggesting proteasome-dependent degradation of ubiquitinated KEAP1.

Several studies have indirectly shown that *AKR1B10* is inducible by NRF2 inducers (Hübner et al., 2009) and is one of the most up-regulated genes when KEAP1 is knocked down (MacLeod et al., 2009), but *AKR1B10* is not an established NRF2 target gene. Therefore, we performed single or double knockdowns in HK-2 cells using two pairs of siRNA. At 48 hr after siRNA transfection, we induced the cells with 100 μM of DMF for 24 hr and then measured the AKR1B10 mRNA levels.

The AKR1B10 mRNA level with use of a scrambled siRNA and induced by DMF was 8.37-fold higher than that of a noninduced scrambled-siRNA control. Knocking down NRF1 with either targeting siRNA prior to DMF induction resulted in a 30% reduction in the fumarate-induced AKR1B10 mRNA (5.87-fold increase relative to noninduced scrambled control). More impressively, a similar experiment with NRF2-targeting siRNA showed an 84% decrease in the DMF-induced AKR1B10 mRNA (1.35-fold increase relative to noninduced scrambled control). Knocking down both NRF1 and NRF2 totally abolished *AKR1B10* transcription induced by DMF (Figure 6E). These results showed that both NRF1 and NRF2 can drive the expression of *AKR1B10*, with NRF2 playing a more important role. This agrees with published work in HaCaT keratinocytes showing that AKR1B10 is up-regulated upon KEAP1 knockdown and that the effect is abolished upon NRF2 knockdown (MacLeod et al., 2009).

We also identified an ARE consensus sequence at location chr7:134,209,958-134,209,968 (Feb. 2009 [GRCh37/hg19]) within the enhancer region of the *AKR1B10* gene. We used chromatin immunoprecipitation (ChIP) in UOK-262, DMF-induced HK-2, and DMF-induced HEK293 cells to pull down DNA fragments that were bound to NRF1 and NRF2. Using PCR primers that specifically amplify DNA fragments from location chr7:134,209,852-134,210,018, which cover the putative enhancer box, we found that the DNA pulled down with both NRF1 and NRF2 was enriched with fragments from that location (Figure S5D). A promoter reporter assay using pGL4-based reporter constructs carrying a putative *AKR1B10* promoter (including or excluding the ARE sequence) also confirmed that the identified ARE is inducible by FH knockdown (Figure 6F).

AKR1B10 Is Specifically Higher in PRCC2

We used immunohistochemical (IHC) staining to detect AKR1B10 in normal kidney tissue, type 1 papillary renal cell carcinoma (PRCC1), and PRCC2; the tissues were from three cohorts of patients in Singapore, Ohio, and Michigan. In accord with our genomic data, the AKR1B10 level was specifically increased in PRCC2 in all three cohorts (Figures 7A–7G) and in HLRCC samples (Figure 7H). These results imply that AKR1B10 could be used as a diagnostic marker to differentiate HLRCC and

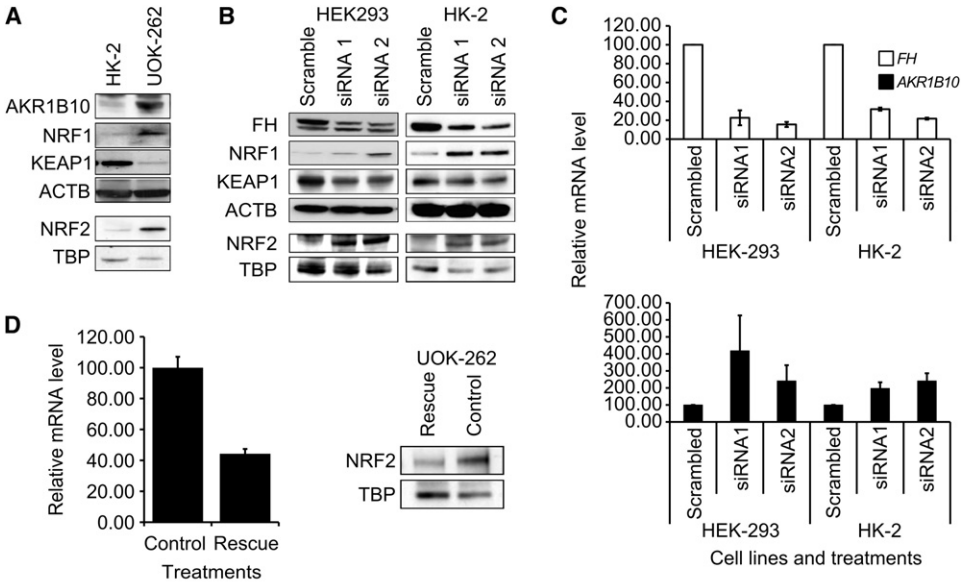

E

Cell lines	Intracellular fumarate level [μmol/g protein] ± standard deviation	FH activity [(ΔA450nm/minute)/mg protein] ± standard deviation
UOK-262 (Parental)	72.80 ± 0.72	0.212 ± 0.003
HEK-293 (Parental)	14.91 ± 0.27	0.644 ± 0.011
HK-2 (Parental)	4.43 ± 0.09	0.692 ± 0.011
UOK-262 (Transduction control)	61.10 ± 1.45	0.160 ± 0.040
UOK-262 (*FH* knock-in)	41.30 ± 1.28	0.344 ± 0.010
HEK-293 (Scrambled siRNA control)	15.49 ± 0.36	
HEK-293 (siRNA against *FH*)	17.27 ± 0.03	
HK-2 (Scrambled siRNA control)	4.56 ± 0.03	
HK-2 (siRNA against *FH*)	8.81 ± 0.19	

Figure 5. AKR1B10 mRNA Increased on Reduction in FH Level or Increase of Intracellular Fumarate

(A) Western blot showing the AKR1B10, NRF1, and KEAP1 levels in whole cell lysates and the NRF2 level in nuclear extracts of HK-2 and UOK-262 cells. β-actin (ACTB) and TATA box binding protein (TBP) were loading controls.

(B) Western blot showing FH, NRF1, and KEAP1 levels in whole cell lysates and NRF2 level in nuclear extracts of the HK-2 and HEK293 cells transfected with scrambled siRNA or siRNA1 and 2 targeting *FH*.

(C) Quantitative reverse transcription PCR showing the relative AKR1B10 mRNA increase upon siRNA-mediated knockdown of FH. Error bars represent SD.

(D) Right: Western blot of nuclear extracts from rescued and control cells shows a decrease in NRF2 in rescued cells; TBP was loading control. Left: qRT-PCR showing the relative AKR1B10 mRNA decrease upon reexpression of wild-type *FH* (Rescue) in UOK-262 cells. Control cells were transduced with empty vector. Error bars represent SD.

(E) Intracellular fumarate level and FH activity in study cell lines. Intracellular fumarate was much higher in UOK-262 relative to HK-2 and HEK293 cells. Reexpression of wild-type *FH* in UOK-262 also decreased intracellular fumarate. RNAi-mediated knockdown of FH in HK-2 and HEK293 cells increased intracellular fumarate levels. See also Figure S4.

PRCC2 from the more indolent PRCC1. Expression of the classic NRF2 target gene *NQO1* was specifically up-regulated in HLRCC and PRCC2, but showed only focal staining in normal kidney tissues (Figures 7I–7K); NQO1 has been shown to be specifically up-regulated in HLRCC (Linehan et al., 2007). IHC staining of NRF2 was also more intense in HLRCC samples (Figure S6). Hence, specific overexpression of *AKR1B10* and *NQO1*, as well as higher NRF2 levels in both HLRCC and PRCC2, support our finding that overexpression of ARE-controlled genes is a biochemical feature shared between HLRCC and PRCC2.

DISCUSSION

Hereditary forms of kidney cancer have provided important insights into the pathways driving the development of kidney cancer subtypes, but the biochemical features shared by the hereditary and sporadic forms of PRCC2 have remained elusive. Herein we report the overexpression of ARE-controlled genes as a biochemical feature shared by both hereditary and sporadic PRCC2.

The ARE controls a battery of phase II biotransformation enzymes (Chan et al., 2001; McMahon et al., 2001). It is inducible by many thiol-reactive compounds and by systemic conditions such as hyperglycemia that produce advanced glycation products (He et al., 2010; Sango et al., 2006). As such, the expression of ARE-controlled genes is high in liver, where xenobiotic detoxification takes place, as well as in rare isolated cases of normal kidney samples (result not shown).

Our results suggest that in HLRCC, the induction of ARE-controlled genes is mediated by fumarate, an electrophile that

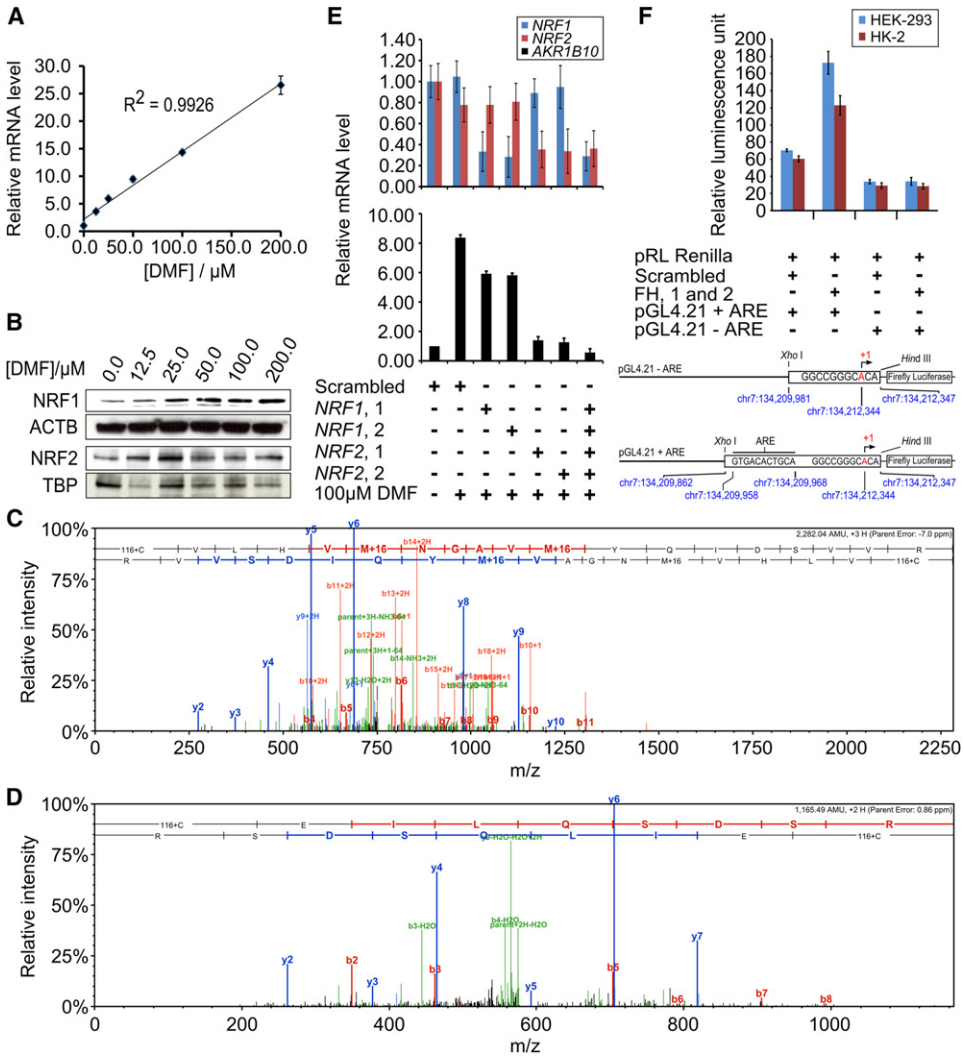

Figure 6. Fumarate Stabilization of NRF1 and NRF2

(A) qRT-PCR of AKR1B10 mRNA in cells exposed to DMF; error bars represent SD.

(B) Western blots of whole cell lysates show that cellular NRF1 increased in a dose-dependent manner with increasing concentration of DMF, as did NRF2 in the nuclear lysate. ACTB and TBP were loading controls.

(C) Mass spectrum showing Cys-151 of human KEAP1 modified by a 2-succinyl group. (Fragmentation tables of the mass spectrum together and of a nonsuccinated peptide are in Table S6).

(D) Mass spectrum showing Cys-288 of human KEAP1 was modified by a 2-succinyl group (fragmentation tables are in Table S6).

(E) qRT-PCR of NRF1, NRF2, and AKR1B10 mRNA in HK-2 cells subjected to single or double *NRF1*/*NRF2* gene knockdown followed by induction with 100 μM DMF for 24 hr. Error bars represent SD.

(F) Promoter reporter assay using Dual-Glo Luciferase Assay System (Promega) with pGL4.21 vector showed that the ARE at location chr7:134,209,958-chr7:134,209,968 was inducible by siRNA knockdown (upper panel). Error bars represent SD pRL-TK was a transfection normalization control. Lower panel shows the DNA fragments cloned into the pGL4.21 vectors. Chromosomal locations are shown in blue; red indicates the *AKR1B10* transcription start site (chr7:134,212,344). The ARE sequence is also shown. See also Figure S5 and Table S6.

can react with a cysteine sulfhydryl through a nucleophilic addition reaction (Alderson et al., 2006). This posttranslational modification has been demonstrated (Blatnik et al., 2008; Frizzell et al., 2010; Frizzell et al., 2009; Nagai et al., 2007). Therefore, it is likely that fumarate reacts with Cys-151 and Cys-288 of KEAP1, leading to stabilization of NRF2, which drives the transcription of ARE-controlled genes. This mechanism also explains the observation that fumarate (and its derivative) but not succinate can induce an increase in NQO1 and glutathione-*S*-transferase (GST) activities in rodent cells and tissues (Spencer et al., 1990).

In PRCC2, the expression phenotype suggests that somatic mutation of genes involving electrophilic metabolic intermediates could contribute to the increased expression of ARE-controlled genes. Furthermore, loss- or gain-of-function mutations to *KEAP1* or *NRF2*, respectively, could have the same effect. Several examples of ARE-controlled gene induction by electrophilic metabolites include metabolites from fatty acid

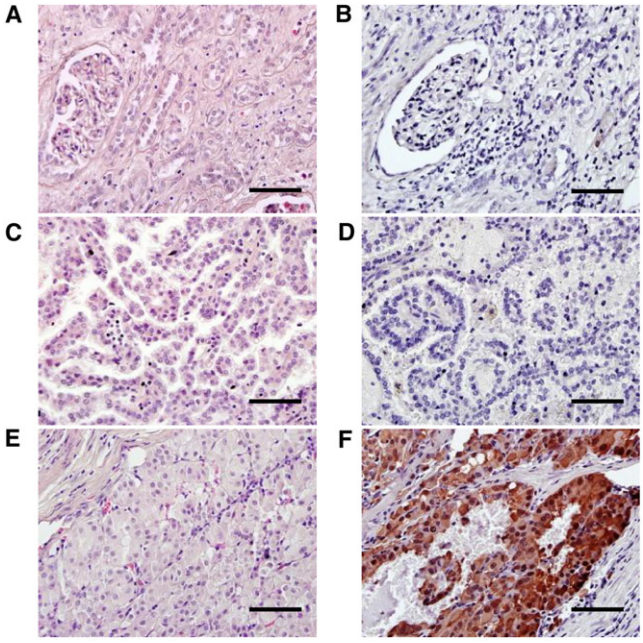

G

Cohorts	Subtypes	Positive Staining / Total Cases
Singapore	1	0/14
	2	8/9
Michigan	1	0/27
	2	18/21
Ohio	1	2/10
	2	9/11

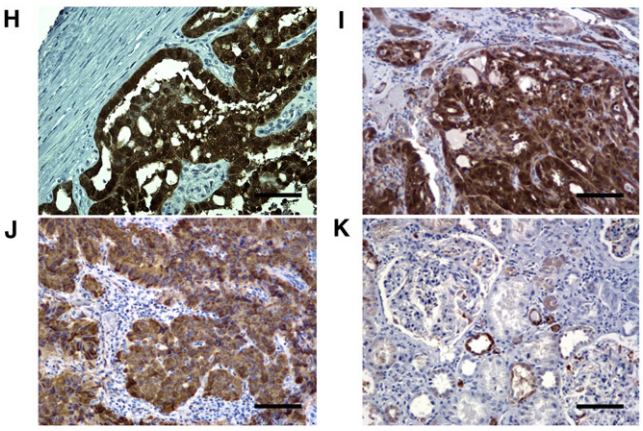

Figure 7. AKR1B10 Protein Increase in PRCC2

(A–F) H&E (A, C, and E) and AKR1B10 IHC staining (B, D, and F) of normal kidney (A and B), PRCC1 (C and D), and PRCC2 (E and F).

(G) The number of positive AKR1B10 IHC stains in three cohorts providing papillary RCC samples. The specificity and sensitivity of AKR1B10 staining in differentiating type 2 from type 1 tumor were consistent in all three cohorts.

(H) AKR1B10 staining in an HLRCC sample (scale bar = 0.1 mm).

(I–K) NQO1 staining in HLRCC, PRCC2, and normal kidney samples (scale bar = 0.1 mm). See also Figure S6.

metabolism (Gao et al., 2007; Siow et al., 2007; Wang et al., 2009), polyamine metabolism (Kwak et al., 2003), and L-tryptophan metabolism (Pae et al., 2006). Loss-of-function mutations and epigenetic silencing of metabolic enzymes that cause electrophilic metabolites to accumulate have been associated with increased cancer risk. For example, mutation of fumarylacetoacetate hydrolase, causing accumulation of fumarylacetoacetate, is associated with hepatocellular carcinoma (Russo and O'Regan, 1990). Epigenetic silencing of 3-hydroxyanthranilate-3,4-dioxygenase (*HAAO*), which oxidizes the electrophilic L-tryptophan metabolite 3-hydroxyanthranilic acid, is found in endometrial and ovarian carcinoma (Huang et al., 2009; Huang et al., 2010). Hence, we propose that reduced KEAP1 function causes the increased expression of ARE-controlled genes in both HLRCC and PRCC2 (Figure 8).

Reduced KEAP1 function will produce NRF2 stabilization and the overexpression of ARE-controlled genes, which neutralize oxidative stresses and thus provide a growth advantage (reviewed in Lau et al., 2008). *KEAP1*-inactivating and *NRF2*-activating mutations are found in many lung cancers (Ohta et al., 2008; Shibata et al., 2008; Singh et al., 2006; Wang et al., 2008), and *KEAP1*-inactivating mutations are markers of poor prognosis in other cancers (Nioi and Nguyen, 2007). The abilities of ARE-controlled genes to neutralize oxidative stress have also been shown in cells that harbor mutations in genes that produce electrophilic intermediates (Lau et al., 2008).

In this study, we demonstrated that increased *AKR1B10* expression occurs with only a moderate reduction in the FH level, suggesting that in the context of HLRCC, the stabilization of NRF2 occurs prior to neoplasia. This is particularly important in HLRCC, which depends on glucose as the primary energy source, creating high ROS stress (Sudarshan et al., 2009). NRF2 stabilization may enable precancerous cells to endure the oxidative stresses of subsequent transforming events. Alternatively, deregulation of the KEAP1-NRF2 axis introduces another mechanism for stabilizing HIF-α in HLRCC. The thioredoxin reductase/thioredoxin pathway can stabilize HIF-α through PKCδ (Koshikawa et al., 2009; Malec et al., 2010), a mechanism consistent with previous work (Sudarshan et al., 2009). Hence, this pathway, together with direct inhibition of HIF prolyl hydroxylase by fumarate and succinate, could contribute to the elevated HIF-α level in HLRCC. Finally, KEAP1 is a negative regulator of NFκB: KEAP1 E3 ligase activity is involved in ubiquitination of IKKβ (Lee et al., 2009). Therefore, our finding predicts activation of the NFκB pathway in HLRCC and PRCC2.

The identification of KEAP1-NRF2 deregulation suggests that a single therapeutic intervention might be possible for both HLRCC and PRCC2 in terms of ARE-controlled genes. One possibility is directly inhibiting genes such as *AKR1B10* to reduce cellular detoxification capability. siRNA-mediated knockdown of AKR1B10 in HLRCC cell lines has halted proliferation (preliminary results, data not shown). Thioredoxin reductase I is also a potential therapeutic target (Holmgren and Lu, 2010). The TXNRD1 inhibitor cisplatin is effective in controlling HLRCC cell growth in vitro and in vivo through increasing the cellular ROS level (Sourbier et al., 2010). Thioredoxin reductase could also be targeted using curcumin or dinitrochlorobenzene (DNCB), which can modify the enzyme to enhance its NADPH oxidase activity and hence elevate ROS to a level not tolerable by the cancer cells (Holmgren and Lu, 2010). Incidentally, both in vitro and in vivo studies have shown that the proteosome inhibitor bortezomib, which inhibits NFκB (Kashkar et al., 2007), can effectively reduce HLRCC cell proliferation (Sourbier et al., 2010). All of these are potential treatment strategies

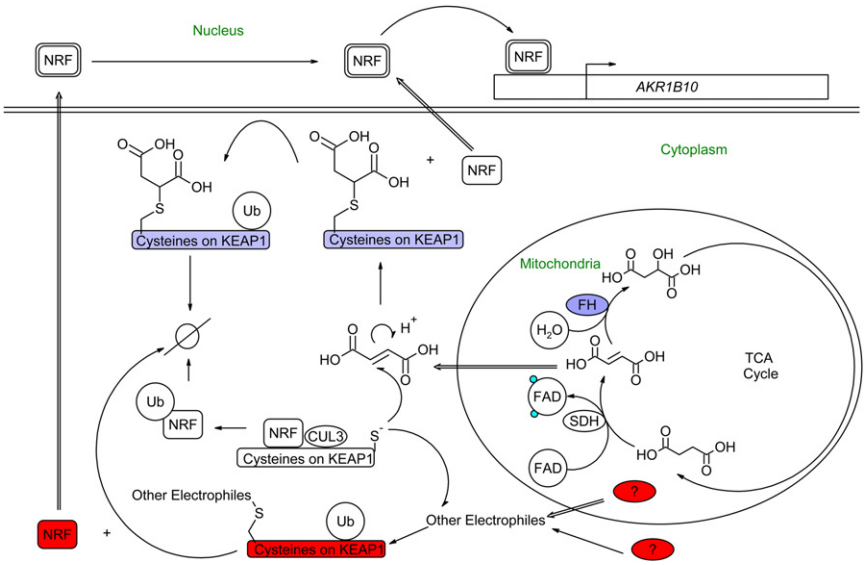

Figure 8. HLRCC and PRCC2 Converge at the Regulation of Genes Controlled by ARE

Diagram shows possible consequences of the loss of FH function in HLRCC (violet) and the mechanism of *AKR1B10* overexpression in PRCC2 (red). Fumarate that accumulates because of *FH* mutation is translocated into the cytosol, where it reacts with cysteines of KEAP1 and alters the KEAP1 conformation, releasing NRF1 and NRF2 from the cytoskeleton. Free NRF1 and NRF2 can then be translocated to the nucleus, where they could bind to ARE and drive the expression of genes such as *AKR1B10* and *NQO1*.

designed specifically for the aggressive type 2 papillary RCC, both hereditary and sporadic.

EXPERIMENTAL PROCEDURES

Clinical Samples

All clinical samples in this study were collected with patient consent and under approval from the Institutional Review Boards (IRBs) of the Van Andel Research Institute, Singapore General Hospital, National Cancer Centre Singapore, Cleveland Clinic, and Le Kremlin-Bicêtre University Hospital, France. Fresh tissue samples were collected from surgery, immediately snap-frozen in liquid nitrogen, and kept in a −80°C freezer for subsequent use. Formalin-fixed, paraffin-embedded tissue blocks were retrieved from the pathology departments of the involved institutions. Blood samples were collected with patient consent, using EDTA vacutainers.

The demographics and mutation status for the five HLRCC samples used in this study are summarized in Table S2.

Identification of Differentially Expressed Genes (Discriminant Gene Analysis)

Genes that were differentially expressed twofold or more between tumor and control tissues were identified using LIMMA (Smyth, 2005). Raw p values were corrected for multiple testing using the false discovery rate method (Benjamini and Hochberg, 1995); differences of less than 0.05 were deemed significant throughout this study.

Parametric Gene Set Analysis

Parametric gene set analysis was performed using the PGSEA package from the Bioconductor repository (Furge et al., 2007). To enable a simple comparison of relative FH signature enrichment, we combined the calculated t-statistics for each of the up- and down-regulated portions of the signature by adding the t-statistic from the up-regulated portion to the additive inverse of the t-statistic for the down-regulated portion. The resulting t-statistic derivative was termed "FH signature enrichment (z-score)."

Cis-Acting Element Prediction

This algorithm is described in detail in Supplemental Experimental Procedures. The workflow of this algorithm is summarized in Figure S2. Briefly, the algorithm looks for genes that share same expression pattern with the gene under interrogation (*AKR1B10*) in three different data sets, and used the identified genes in a modified gene set enrichment analysis to predict *cis*-acting element that control the transcription of the gene under interrogation.

Treatment with DMF

For DMF exposure experiments, cells were seeded onto 10-cm cell culture dishes at about 70% confluence and acclimated to the cell culture conditions for 24 hr. Then the cell culture medium was replaced with medium premixed with a specified concentration of DMF. Cells were cultured in this medium for 24 hr before harvesting for the preparation of whole cell lysate, nuclear extract, or total RNA.

Determination of Intracellular Fumarate Concentration

Total cellular metabolites were extracted from cells cultured in a six-well plate using perchloric acid extraction (Supplemental Experimental Procedures). The concentration of fumarate was determined using a commercial kit (Fumarate assay kit, BioVision).

Expression and Purification of HA-Tagged Human KEAP1 from siRNA-Treated HEK293 Cells

HEK293 cells cultured in 10 cm^2 cell culture dishes were treated with siRNA against FH or a scrambled control. On the second day after siRNA transfection, pcDNA3 carrying the open reading frame coding for HA-tagged human KEAP1 (pcDNA3-HA2-KEAP1) (Furukawa and Xiong, 2005) was transfected into the cells using Lipofectamine 2000 (Invitrogen). Cells were cultured for an additional 52 hr before being harvested for immunoprecipitation.

Cell harvesting and immunoprecipitation of HA-tagged KEAP1 used an anti-HA immunoprecipitation kit (Sigma) according to the manufacturer's protocol.

For treatment with MG132 (proteasome inhibitor), cells were incubated for 4 hr with fresh medium containing either 10 μM of MG132 or vehicle (0.001% DMSO) at 48 hr after transfection of pcDNA3-HA2-KEAP1.

Samples Used in Liquid Chromatography-Tandem Mass Spectrometry (LC-MS/MS)

Immunoprecipitated HA-tagged human KEAP1 expressed in HEK293 cells pretransfected with either *FH* targeting or scrambled siRNA was resolved in a 4%–20% SDS polyacrylamide gel (Bio-Rad). Protein was visualized by Coomassie blue R-250 staining. The resulting protein band of approximately 65 kDa was excised from the gel and used in LC-MS/MS analysis (Supplemental Experimental Procedures).

Lentivirus-Mediated Transgene Knock-In of Wild-Type *FH* into UOK-262 Cells

The open reading frame of *FH* was cloned into pIRES-Puro (Clonetech) downstream of a cytomegalovirus (CMV) promoter. The resulting cassette was then transferred into pENTR1A (Invitrogen) and subsequently transferred into a modified lentivirus vector (see Supplemental Experimental Procedures). The virus was then packaged and used to transduce UOK-262 cells. Cells were harvested on the third day after transduction for qRT-PCR determination of AKR1B10 mRNA, measurement of intracellular fumarate concentration, and

Western blot analysis. Lentivirus packaged from an empty vector (carrying the CMV promoter and the puromycin resistance cassette from pIRES-Puro) was used as a transduction control. A schematic vector map is in the Supplemental Experimental Procedures section.

ACCESSION NUMBER

Microarray data generated in this study have been deposited at the NCBI Gene Expression Omnibus, accession number GSE26574.

SUPPLEMENTAL INFORMATION

Supplemental Information includes six figures, six tables, and Supplemental Experimental Procedures and may be found with this article online at doi:10.1016/j.ccr.2011.08.024.

ACKNOWLEDGMENTS

This paper is dedicated to the memory of Thean-Poh Ooi.

We thank Sabrina Noyes for administrative support and David Nadziejka for technical editing. We acknowledge the Van Andel Research Foundation, the Singapore Millennium Foundation, and Fondation IGR & INCa (PNES Rein and Centre Expert National Cancers Rares PREDIR) for funding. A.O., K.F., and B.T. designed the study; A.O. performed all experiments, bioinformatics, and data analysis; J.C.W. and D.R. performed IHC staining; D.P. performed microarray experiments; D.W. performed tandem mass spectrometry; and X.J.Y. and M.Z. performed histological evaluation. B.T., Z.Z., M.Z., M.H.T., B.H.W., V.P.T., P.H.T., B.G., V.M., and S.R. provided samples and clinical data. A.O. and K.F. prepared the manuscript. Mass spectrometry and data analysis were performed in the Michigan State University, Proteomic Core Facility.

Received: December 22, 2010
Revised: June 4, 2011
Accepted: August 30, 2011
Published: October 17, 2011

REFERENCES

Alam, N.A., Rowan, A.J., Wortham, N.C., Pollard, P.J., Mitchell, M., Tyrer, J.P., Barclay, E., Calonje, E., Manek, S., Adams, S.J., et al. (2003). Genetic and functional analyses of FH mutations in multiple cutaneous and uterine leiomyomatosis, hereditary leiomyomatosis and renal cancer, and fumarate hydratase deficiency. Hum. Mol. Genet. *12*, 1241–1252.

Alderson, N.L., Wang, Y., Blatnik, M., Frizzell, N., Walla, M.D., Lyons, T.J., Alt, N., Carson, J.A., Nagai, R., Thorpe, S.R., and Baynes, J.W. (2006). S-(2-Succinyl)cysteine: a novel chemical modification of tissue proteins by a Krebs cycle intermediate. Arch. Biochem. Biophys. *450*, 1–8.

Bellacosa, A., Godwin, A.K., Peri, S., Devarajan, K., Caretti, E., Vanderveer, L., Bove, B., Slater, C., Zhou, Y., Daly, M., et al. (2010). Altered gene expression in morphologically normal epithelial cells from heterozygous carriers of BRCA1 or BRCA2 mutations. Cancer Prev Res (Phila) *3*, 48–61.

Benjamini, Y., and Hochberg, Y. (1995). Controlling the false discovery rate: a practical and powerful approach to multiple testing. J. R. Stat. Soc. B *57*, 289–300.

Blatnik, M., Thorpe, S.R., and Baynes, J.W. (2008). Succination of proteins by fumarate: mechanism of inactivation of glyceraldehyde-3-phosphate dehydrogenase in diabetes. Ann. N Y Acad. Sci. *1126*, 272–275.

Carvajal-Carmona, L.G., Alam, N.A., Pollard, P.J., Jones, A.M., Barclay, E., Wortham, N., Pignatelli, M., Freeman, A., Pomplun, S., Ellis, I., et al. (2006). Adult leydig cell tumors of the testis caused by germline fumarate hydratase mutations. J. Clin. Endocrinol. Metab. *91*, 3071–3075.

Chan, K., Han, X.D., and Kan, Y.W. (2001). An important function of Nrf2 in combating oxidative stress: detoxification of acetaminophen. Proc. Natl. Acad. Sci. USA *98*, 4611–4616.

Dahia, P.L., Ross, K.N., Wright, M.E., Hayashida, C.Y., Santagata, S., Barontini, M., Kung, A.L., Sanso, G., Powers, J.F., Tischler, A.S., et al. (2005). A HIF1alpha regulatory loop links hypoxia and mitochondrial signals in pheochromocytomas. PLoS Genet. *1*, 72–80.

Frizzell, N., Lima, M., and Baynes, J.W. (2010). Succination of proteins in diabetes. Free Radic. Res. *45*, 101–109.

Frizzell, N., Rajesh, M., Jepson, M.J., Nagai, R., Carson, J.A., Thorpe, S.R., and Baynes, J.W. (2009). Succination of thiol groups in adipose tissue proteins in diabetes: succination inhibits polymerization and secretion of adiponectin. J. Biol. Chem. *284*, 25772–25781.

Furge, K.A., Tan, M.H., Dykema, K., Kort, E., Stadler, W., Yao, X., Zhou, M., and Teh, B.T. (2007). Identification of deregulated oncogenic pathways in renal cell carcinoma: an integrated oncogenomic approach based on gene expression profiling. Oncogene *26*, 1346–1350.

Furukawa, M., and Xiong, Y. (2005). BTB protein Keap1 targets antioxidant transcription factor Nrf2 for ubiquitination by the Cullin 3-Roc1 ligase. Mol. Cell. Biol. *25*, 162–171.

Gao, L., Wang, J., Sekhar, K.R., Yin, H., Yared, N.F., Schneider, S.N., Sasi, S., Dalton, T.P., Anderson, M.E., Chan, J.Y., et al. (2007). Novel n-3 fatty acid oxidation products activate Nrf2 by destabilizing the association between Keap1 and Cullin3. J. Biol. Chem. *282*, 2529–2537.

Hayes, J.D., and McMahon, M. (2001). Molecular basis for the contribution of the antioxidant responsive element to cancer chemoprevention. Cancer Lett. *174*, 103–113.

Holmgren, A., and Lu, J. (2010). Thioredoxin and thioredoxin reductase: current research with special reference to human disease. Biochem. Biophys. Res. Commun. *396*, 120–124.

Hsieh, T.C., Lu, X., Wang, Z., and Wu, J.M. (2006). Induction of quinone reductase NQO1 by resveratrol in human K562 cells involves the antioxidant response element ARE and is accompanied by nuclear translocation of transcription factor Nrf2. Med. Chem. *2*, 275–285.

Huang, Y.W., Jansen, R.A., Fabbri, E., Potter, D., Liyanarachchi, S., Chan, M.W., Liu, J.C., Crijns, A.P., Brown, R., Nephew, K.P., et al. (2009). Identification of candidate epigenetic biomarkers for ovarian cancer detection. Oncol. Rep. *22*, 853–861.

Huang, Y.W., Luo, J., Weng, Y.I., Mutch, D.G., Goodfellow, P.J., Miller, D.S., and Huang, T.H. (2010). Promoter hypermethylation of CIDEA, HAAO and RXFP3 associated with microsatellite instability in endometrial carcinomas. Gynecol. Oncol. *117*, 239–247.

Hübner, R.H., Schwartz, J.D., De Bishnu, P., Ferris, B., Omberg, L., Mezey, J.G., Hackett, N.R., and Crystal, R.G. (2009). Coordinate control of expression of Nrf2-modulated genes in the human small airway epithelium is highly responsive to cigarette smoking. Mol. Med. *15*, 203–219.

Isaacs, J.S., Jung, Y.J., Mole, D.R., Lee, S., Torres-Cabala, C., Chung, Y.L., Merino, M., Trepel, J., Zbar, B., Toro, J., et al. (2005). HIF overexpression correlates with biallelic loss of fumarate hydratase in renal cancer: novel role of fumarate in regulation of HIF stability. Cancer Cell *8*, 143–153.

Ivan, M., Kondo, K., Yang, H., Kim, W., Valiando, J., Ohh, M., Salic, A., Asara, J.M., Lane, W.S., and Kaelin, W.G., Jr. (2001). HIFalpha targeted for VHL-mediated destruction by proline hydroxylation: implications for O2 sensing. Science *292*, 464–468.

Kashkar, H., Deggerich, A., Seeger, J.M., Yazdanpanah, B., Wiegmann, K., Haubert, D., Pongratz, C., and Krönke, M. (2007). NF-kappaB-independent down-regulation of XIAP by bortezomib sensitizes HL B cells against cytotoxic drugs. Blood *109*, 3982–3988.

Kiuru, M., and Launonen, V. (2004). Hereditary leiomyomatosis and renal cell cancer (HLRCC). Curr. Mol. Med. *4*, 869–875.

Koivunen, P., Hirsilä, M., Remes, A.M., Hassinen, I.E., Kivirikko, K.I., and Myllyharju, J. (2007). Inhibition of hypoxia-inducible factor (HIF) hydroxylases by citric acid cycle intermediates: possible links between cell metabolism and stabilization of HIF. J. Biol. Chem. *282*, 4524–4532.

Koshikawa, N., Hayashi, J., Nakagawara, A., and Takenaga, K. (2009). Reactive oxygen species-generating mitochondrial DNA mutation up-regulates hypoxia-inducible factor-1alpha gene transcription via

phosphatidylinositol 3-kinase-Akt/protein kinase C/histone deacetylase pathway. J. Biol. Chem. *284*, 33185–33194.

Kwak, M.K., Kensler, T.W., and Casero, R.A., Jr. (2003). Induction of phase 2 enzymes by serum oxidized polyamines through activation of Nrf2: effect of the polyamine metabolite acrolein. Biochem. Biophys. Res. Commun. *305*, 662–670.

Lau, A., Villeneuve, N.F., Sun, Z., Wong, P.K., and Zhang, D.D. (2008). Dual roles of Nrf2 in cancer. Pharmacol. Res. *58*, 262–270.

Launonen, V., Vierimaa, O., Kiuru, M., Isola, J., Roth, S., Pukkala, E., Sistonen, P., Herva, R., and Aaltonen, L.A. (2001). Inherited susceptibility to uterine leiomyomas and renal cell cancer. Proc. Natl. Acad. Sci. USA *98*, 3387–3392.

Lee, D.F., Kuo, H.P., Liu, M., Chou, C.K., Xia, W., Du, Y., Shen, J., Chen, C.T., Huo, L., Hsu, M.C., et al. (2009). KEAP1 E3 ligase-mediated downregulation of NF-kappaB signaling by targeting IKKbeta. Mol. Cell *36*, 131–140.

Lehtonen, H.J., Kiuru, M., Ylisaukko-Oja, S.K., Salovaara, R., Herva, R., Koivisto, P.A., Vierimaa, O., Aittomäki, K., Pukkala, E., Launonen, V., and Aaltonen, L.A. (2006). Increased risk of cancer in patients with fumarate hydratase germline mutation. J. Med. Genet. *43*, 523–526.

Linehan, W.M., Bratslavsky, G., Pinto, P.A., Schmidt, L.S., Neckers, L., Bottaro, D.P., and Srinivasan, R. (2010). Molecular diagnosis and therapy of kidney cancer. Annu. Rev. Med. *61*, 329–343.

Linehan, W.M., Pinto, P.A., Srinivasan, R., Merino, M., Choyke, P., Choyke, L., Coleman, J., Toro, J., Glenn, G., Vocke, C., et al. (2007). Identification of the genes for kidney cancer: opportunity for disease-specific targeted therapeutics. Clin. Cancer Res. *13*, 671s–679s.

MacLeod, A.K., McMahon, M., Plummer, S.M., Higgins, L.G., Penning, T.M., Igarashi, K., and Hayes, J.D. (2009). Characterization of the cancer chemopreventive NRF2-dependent gene battery in human keratinocytes: demonstration that the KEAP1-NRF2 pathway, and not the BACH1-NRF2 pathway, controls cytoprotection against electrophiles as well as redox-cycling compounds. Carcinogenesis *30*, 1571–1580.

Malec, V., Gottschald, O.R., Li, S., Rose, F., Seeger, W., and Hänze, J. (2010). HIF-1 alpha signaling is augmented during intermittent hypoxia by induction of the Nrf2 pathway in NOX1-expressing adenocarcinoma A549 cells. Free Radic. Biol. Med. *48*, 1626–1635.

McMahon, M., Itoh, K., Yamamoto, M., Chanas, S.A., Henderson, C.J., McLellan, L.I., Wolf, C.R., Cavin, C., and Hayes, J.D. (2001). The Cap'n'Collar basic leucine zipper transcription factor Nrf2 (NF-E2 p45-related factor 2) controls both constitutive and inducible expression of intestinal detoxification and glutathione biosynthetic enzymes. Cancer Res. *61*, 3299–3307.

Molina, A.M., Feldman, D.R., Ginsberg, M.S., Kroog, G., Tickoo, S.K., Jia, X., Georges, M., Patil, S., Baum, M.S., Reuter, V.E., and Motzer, R.J. (2010). Phase II trial of sunitinib in patients with metastatic non-clear cell renal cell carcinoma. Invest. New Drugs. [Epub ahead of print].

Nagai, R., Brock, J.W., Blatnik, M., Baatz, J.E., Bethard, J., Walla, M.D., Thorpe, S.R., Baynes, J.W., and Frizzell, N. (2007). Succination of protein thiols during adipocyte maturation: a biomarker of mitochondrial stress. J. Biol. Chem. *282*, 34219–34228.

Nioi, P., and Nguyen, T. (2007). A mutation of Keap1 found in breast cancer impairs its ability to repress Nrf2 activity. Biochem. Biophys. Res. Commun. *362*, 816–821.

O'Flaherty, L., Adam, J., Heather, L.C., Zhdanov, A.V., Chung, Y.L., Miranda, M.X., Croft, J., Olpin, S., Clarke, K., Pugh, C.W., et al. (2010). Dysregulation of hypoxia pathways in fumarate hydratase-deficient cells is independent of defective mitochondrial metabolism. Hum. Mol. Genet. *19*, 3844–3851.

Ohta, T., Iijima, K., Miyamoto, M., Nakahara, I., Tanaka, H., Ohtsuji, M., Suzuki, T., Kobayashi, A., Yokota, J., Sakiyama, T., et al. (2008). Loss of Keap1 function activates Nrf2 and provides advantages for lung cancer cell growth. Cancer Res. *68*, 1303–1309.

Ohtsuji, M., Katsuoka, F., Kobayashi, A., Aburatani, H., Hayes, J.D., and Yamamoto, M. (2008). Nrf1 and Nrf2 play distinct roles in activation of antioxidant response element-dependent genes. J. Biol. Chem. *283*, 33554–33562.

Pae, H.O., Oh, G.S., Lee, B.S., Rim, J.S., Kim, Y.M., and Chung, H.T. (2006). 3-Hydroxyanthranilic acid, one of L-tryptophan metabolites, inhibits monocyte chemoattractant protein-1 secretion and vascular cell adhesion molecule-1 expression via heme oxygenase-1 induction in human umbilical vein endothelial cells. Atherosclerosis *187*, 274–284.

Pollard, P., Wortham, N., Barclay, E., Alam, A., Elia, G., Manek, S., Poulsom, R., and Tomlinson, I. (2005a). Evidence of increased microvessel density and activation of the hypoxia pathway in tumours from the hereditary leiomyomatosis and renal cell cancer syndrome. J. Pathol. *205*, 41–49.

Pollard, P.J., Brière, J.J., Alam, N.A., Barwell, J., Barclay, E., Wortham, N.C., Hunt, T., Mitchell, M., Olpin, S., Moat, S.J., et al. (2005b). Accumulation of Krebs cycle intermediates and over-expression of HIF1alpha in tumours which result from germline FH and SDH mutations. Hum. Mol. Genet. *14*, 2231–2239.

Pollard, P.J., El-Bahrawy, M., Poulsom, R., Elia, G., Killick, P., Kelly, G., Hunt, T., Jeffery, R., Seedhar, P., Barwell, J., et al. (2006). Expression of HIF-1alpha, HIF-2alpha (EPAS1), and their target genes in paraganglioma and pheochromocytoma with VHL and SDH mutations. J. Clin. Endocrinol. Metab. *91*, 4593–4598.

Rachakonda, G., Xiong, Y., Sekhar, K.R., Stamer, S.L., Liebler, D.C., and Freeman, M.L. (2008). Covalent modification at Cys151 dissociates the electrophile sensor Keap1 from the ubiquitin ligase CUL3. Chem. Res. Toxicol. *21*, 705–710.

Russo, P., and O'Regan, S. (1990). Visceral pathology of hereditary tyrosinemia type I. Am. J. Hum. Genet. *47*, 317–324.

Sakurai, A., Nishimoto, M., Himeno, S., Imura, N., Tsujimoto, M., Kunimoto, M., and Hara, S. (2005). Transcriptional regulation of thioredoxin reductase 1 expression by cadmium in vascular endothelial cells: role of NF-E2-related factor-2. J. Cell. Physiol. *203*, 529–537.

Sango, K., Suzuki, T., Yanagisawa, H., Takaku, S., Hirooka, H., Tamura, M., and Watabe, K. (2006). High glucose-induced activation of the polyol pathway and changes of gene expression profiles in immortalized adult mouse Schwann cells IMS32. J. Neurochem. *98*, 446–458.

Shibata, T., Ohta, T., Tong, K.I., Kokubu, A., Odogawa, R., Tsuta, K., Asamura, H., Yamamoto, M., and Hirohashi, S. (2008). Cancer related mutations in NRF2 impair its recognition by Keap1-Cul3 E3 ligase and promote malignancy. Proc. Natl. Acad. Sci. USA *105*, 13568–13573.

Singh, A., Misra, V., Thimmulappa, R.K., Lee, H., Ames, S., Hoque, M.O., Herman, J.G., Baylin, S.B., Sidransky, D., Gabrielson, E., et al. (2006). Dysfunctional KEAP1-NRF2 interaction in non-small-cell lung cancer. PLoS Med. *3*, e420.

Siow, R.C., Ishii, T., and Mann, G.E. (2007). Modulation of antioxidant gene expression by 4-hydroxynonenal: atheroprotective role of the Nrf2/ARE transcription pathway. Redox Rep. *12*, 11–15.

Smyth, G.K. (2005). Limma: linear models for microarray data. In Bioinformatics and Computational Biology Solutions using R and Bioconductor, R. Gentleman, V. Carey, S. Dudoit, R.A. Irizarry, and W. Huber, eds. (New York: Springer), pp. 397–420.

Sourbier, C., Valera-Romero, V., Giubellino, A., Yang, Y., Sudarshan, S., Neckers, L., and Linehan, W.M. (2010). Increasing reactive oxygen species as a therapeutic approach to treat hereditary leiomyomatosis and renal cell carcinoma. Cell Cycle *9*, 4183–4189.

Spencer, S.R., Wilczak, C.A., and Talalay, P. (1990). Induction of glutathione transferases and NAD(P)H:quinone reductase by fumaric acid derivatives in rodent cells and tissues. Cancer Res. *50*, 7871–7875.

Sudarshan, S., Sourbier, C., Kong, H.S., Block, K., Valera Romero, V.A., Yang, Y., Galindo, C., Mollapour, M., Scroggins, B., Goode, N., et al. (2009). Fumarate hydratase deficiency in renal cancer induces glycolytic addiction and hypoxia-inducible transcription factor 1alpha stabilization by glucose-dependent generation of reactive oxygen species. Mol. Cell. Biol. *29*, 4080–4090.

Tomlinson, I.P., Alam, N.A., Rowan, A.J., Barclay, E., Jaeger, E.E., Kelsell, D., Leigh, I., Gorman, P., Lamlum, H., Rahman, S., et al; Multiple Leiomyoma Consortium. (2002). Germline mutations in FH predispose to dominantly inherited uterine fibroids, skin leiomyomata and papillary renal cell cancer. Nat. Genet. *30*, 406–410.

Vanharanta, S., Buchta, M., McWhinney, S.R., Virta, S.K., Peçzkowska, M., Morrison, C.D., Lehtonen, R., Januszewicz, A., Järvinen, H., Juhola, M., et al. (2004). Early-onset renal cell carcinoma as a novel extraparaganglial component of SDHB-associated heritable paraganglioma. Am. J. Hum. Genet. *74*, 153–159.

Vanharanta, S., Pollard, P.J., Lehtonen, H.J., Laiho, P., Sjöberg, J., Leminen, A., Aittomäki, K., Arola, J., Kruhoffer, M., Orntoft, T.F., et al. (2006). Distinct expression profile in fumarate-hydratase-deficient uterine fibroids. Hum. Mol. Genet. *15*, 97–103.

Venugopal, R., and Jaiswal, A.K. (1998). Nrf2 and Nrf1 in association with Jun proteins regulate antioxidant response element-mediated expression and coordinated induction of genes encoding detoxifying enzymes. Oncogene *17*, 3145–3156.

Wang, R., An, J., Ji, F., Jiao, H., Sun, H., and Zhou, D. (2008). Hypermethylation of the Keap1 gene in human lung cancer cell lines and lung cancer tissues. Biochem. Biophys. Res. Commun. *373*, 151–154.

Wang, R., Kern, J.T., Goodfriend, T.L., Ball, D.L., and Luesch, H. (2009). Activation of the antioxidant response element by specific oxidized metabolites of linoleic acid. Prostaglandins Leukot. Essent. Fatty Acids *81*, 53–59.

Yang, Y., Valera, V.A., Padilla-Nash, H.M., Sourbier, C., Vocke, C.D., Vira, M.A., Abu-Asab, M.S., Bratslavsky, G., Tsokos, M., Merino, M.J., et al. (2010). UOK 262 cell line, fumarate hydratase deficient (FH-/FH-) hereditary leiomyomatosis renal cell carcinoma: in vitro and in vivo model of an aberrant energy metabolic pathway in human cancer. Cancer Genet. Cytogenet. *196*, 45–55.

Zhang, D.D., and Hannink, M. (2003). Distinct cysteine residues in Keap1 are required for Keap1-dependent ubiquitination of Nrf2 and for stabilization of Nrf2 by chemopreventive agents and oxidative stress. Mol. Cell. Biol. *23*, 8137–8151.

Zhang, D.D., Lo, S.C., Sun, Z., Habib, G.M., Lieberman, M.W., and Hannink, M. (2005). Ubiquitination of Keap1, a BTB-Kelch substrate adaptor protein for Cul3, targets Keap1 for degradation by a proteasome-independent pathway. J. Biol. Chem. *280*, 30091–30099.

Zhang, Y., Crouch, D.H., Yamamoto, M., and Hayes, J.D. (2006). Negative regulation of the Nrf1 transcription factor by its N-terminal domain is independent of Keap1: Nrf1, but not Nrf2, is targeted to the endoplasmic reticulum. Biochem. J. *399*, 373–385.